# **Article**



# Interplay between environmental yielding and dynamic forcing modulates bacterial growth

Anna M. Hancock<sup>1</sup> and Sujit S. Datta<sup>1,\*</sup>

<sup>1</sup>Chemical and Biological Engineering, Princeton University, Princeton, New Jersey

ABSTRACT Many bacterial habitats—ranging from gels and tissues in the body to cell-secreted exopolysaccharides in biofilms—are rheologically complex, undergo dynamic external forcing, and have unevenly distributed nutrients. How do these features jointly influence how the resident cells grow and proliferate? Here, we address this question by studying the growth of Escherichia coli dispersed in granular hydrogel matrices with defined and highly tunable structural and rheological properties, under different amounts of external forcing imposed by mechanical shaking, and in both aerobic and anaerobic conditions. Our experiments establish a general principle: that the balance between the yield stress of the environment that the cells inhabit,  $\sigma_y$ , and the external stress imposed on the environment,  $\sigma_z$ , modulates bacterial growth by altering transport of essential nutrients to the cells. In particular, when  $\sigma_v < \sigma$ , the environment is easily fluidized and mixed over large scales, providing nutrients to the cells and sustaining complete cellular growth. By contrast, when  $\sigma_v > \sigma$ , the elasticity of the environment suppresses large-scale fluid mixing, limiting nutrient availability and arresting cellular growth. Our work thus reveals a new mechanism, beyond effects that change cellular behavior via local forcing, by which the rheology of the environment may modulate microbial physiology in diverse natural and industrial settings.

SIGNIFICANCE Bacteria often inhabit complex environments whose mechanical properties vary widely; a prominent example is airway mucus, which is a runny solution that is easy to clear from the lungs in healthy humans but a stiff, difficultto-clear viscoelastic gel during disease. How do these changes in environmental rheology influence bacterial growth? Previous studies have documented fascinating ways in which local, cell-scale changes in environmental rheology alter cellular behavior. Here, using experiments on Escherichia coli cells in hydrogel matrices with defined and highly tunable rheological properties, we demonstrate another mechanism by which global, large-scale changes in environmental rheology alter cellular behavior. In particular, we show that when the environment is fragile enough to be fluidized by external forcing, fluid mixing transports essential nutrients to the cells, sustaining their growth. By contrast, when the environment is too tough to be fluidized and mixed, nutrient availability is limited, and cellular growth is arrested. Our work thus establishes a general principle describing how the rheology of the environment may modulate microbial physiology in diverse natural and industrial settings.

#### INTRODUCTION

Many bacterial environments—e.g., gels and tissues inside hosts, subsurface soils and sediments, exopolysaccharides in biofilms and in the environment, activated sludge in sewage treatment plants, and food products (1-13)—are neither perfectly elastic solids nor simple viscous fluids. Instead, they are yield stress materials: they behave as viscoelastic solids when exposed to weak mechanical stresses but flow when the imposed stress exceeds a threshold yield stress  $\sigma_{v}$ . jected to continuous and dynamic external forcing by moving boundaries, fluid flows, and other mechanical stressors. Thus, depending on the balance between the yield stress  $\sigma_{v}$  and external stresses  $\sigma$ , the environments that bacteria inhabit can vary between being solid-like and liquid-like.

Indeed, these habitats are typically not quiescent but are sub-

A familiar example is mucus, which serves as a habitat for both commensal and pathogenic bacteria in diverse animals. In healthy humans, airway mucus is often a runny solution with a small or negligible yield stress; however, many respiratory disorders are characterized by a more concentrated mucus whose yield stress can be as large as tens of pascals (14–17). As a result, the beating cilia that line the airways are less effective at clearing mucus from the lungs—leading,

Submitted December 5, 2023, and accepted for publication March 4, 2024.

\*Correspondence: ssdatta@princeton.edu

Editor: Kerwyn Casey Huang.

https://doi.org/10.1016/j.bpj.2024.03.008

© 2024 Biophysical Society.

This is an open access article under the CC BY-NC-ND license (http:// creativecommons.org/licenses/by-nc-nd/4.0/).



in some cases, to chronic and deadly infections (15,18). Another familiar example is the polymer matrix that encapsulates the cells in a surface-attached biofilm, such as the plaque that we brush off our teeth and the slime that can grow on industrial equipment, medical catheters, and even in our showers. In some cases, this matrix is weak and easily yielded, whereas in others, its yield stress can be as large as thousands of pascals (13,19-24)—which is thought to contribute to biofilm virulence and recalcitrance to treatment. Given that the yield stress of the environments that bacteria inhabit can vary so widely (Table 1), with implications for health, environment, and our everyday lives, we ask: How do changes in yield stress influence bacterial behavior?

Prior research has investigated how other aspects of environmental rheology can influence bacterial behavior via local mechanical forcing (44,45). For example, a growing body of work is elucidating the ways in which individual bacterial cells on 2D planar surfaces sense and respond to changes in surface stiffness and topography via local mechanical forces using their flagella, pili, and membrane proteins (46,47). Other work has shown how 3D confinement of dense, multicellular colonies causes cells to rearrange, slow down growth, and even induce biofilm formation due to large cell-cell contact forces (48–53). In bulk liquids, studies have shown how local stresses generated by fluid flows generated by bacterial swimming alter swimming kinematics (54–59).

Here, we report another, distinct mechanism by which environmental rheology impacts a fundamental aspect of bacterial physiology—cellular growth. By studying Escherichia coli growth inside permeable 3D granular hydrogel matrices, we show that the balance between the yield stress  $\sigma_{v}$  and external stress  $\sigma$ , quantified by the Bingham number Bi  $\equiv \sigma_v / \sigma$  and tuned over a wide range in our experiments, modulates bacterial growth by altering transport of externally supplied essential nutrients to the cells. In particular, when the matrix is fragile enough to be fluidized by shaking (small Bi), mixing transports oxygen from the boundaries of the matrix to the cells; as a result, the bacteria are able to perform aerobic respiration and thereby achieve a high growth yield (60–63). In stark contrast, when the matrix is tough enough to withstand shaking (large Bi), its elasticity hinders mixing; consequently, the majority of the bacteria become oxygen depleted, arresting their growth cycle and greatly diminishing the resultant biomass yield (60–63). Notably, owing to the unique structure of the hydrogel matrices, this transition between continued and arrested growth is not associated with changes in the local mechanical environment encountered by individual cells. Hence, this mechanism by which environmental rheology modulates bacterial physiology—by altering large-scale transport of nutrients—complements other mechanisms that rely on local mechanical forcing instead. Because many bacterial habitats have complex rheological properties, encounter dynamical external forcing, and have heterogeneous nutrient distributions, we anticipate that our findings are applicable to microbial life in diverse natural and industrial settings.

#### **MATERIALS AND METHODS**

# Details of bacterial strains and growth media

Our experiments use two different strains of E. coli, both of strain background W3110, that constitutively express GFPmut2: a motile strain as well as a nonmotile  $\Delta$  flhDC mutant. In all experiments, E. coli are grown in EZ Rich, a defined, rich growth medium (Teknova, Hollister, CA, USA). Our procedure to prepare 100 mL liquid EZ Rich is as follows: mix 10 mL 10× MOPS mixture (M2101), 10 mL 10× ACGU solution (M2103), 20 mL 5× Supplement EZ solution (M2104), and 1 mL 0.132 M potassium phosphate dibasic solution (M2102) in 58 mL ultrapure Milli-Q water. We then autoclave this mixture and add 1 mL sterile 20% aqueous glucose solution once the mixture has cooled.

### Preparing granular hydrogel matrices

We use dense packings of hydrogel grains ("microgels") as growth matrices for bacteria (Fig. 1 A). A useful feature of such matrices is that they have highly tunable yield stresses comparable to those characterizing natural bacterial environments (Table 1; as detailed further below). Each matrix is prepared by dispersing dry granules of internally cross-linked microgels made of biocompatible acrylic acid-alkyl acrylate copolymers (Carbomer 980; Lubrizol, Wickliffe, OH, USA) in liquid EZ Rich. The granules absorb the liquid until their elasticity prevents further swelling. We ensure a homogeneous dispersion of swollen microgels by mixing for at least 12 h using either magnetic stirring or a rotary mixer and adjust the final pH to 7.4 by adding 10 M NaOH. The cells are then uniformly dispersed in the liquid phase in between the microgels and their growth monitored using spectroscopy, as described further below.

TABLE 1 Order of magnitude estimates of rheological parameters characterizing bacterial environments in nature and in this study

Environment	Yield stress $\sigma_y$ (Pa)	External stress $\sigma$ (Pa)	$\mathrm{Bi}\!\equiv\!\sigma_{\mathrm{y}}/\sigma$	References
This study: granular hydrogel matrix	$\ll 10^{-2} - 10^2$	0 - 1	$\ll 10^{-2} - \gg 10^2$	this study, (25–27)
Lung mucus: healthy	$10^{-1} - 10$	$10^{-4} - 10^{2}$	$10^{-3} - 10^{5}$	(14–17, 28–38)
Lung mucus: cystic fibrosis	$10^{-1} - 10^2$	$10^{-4} - 10^{2}$	$10^{-3} - 10^{6}$	(14–16, 28–38)
Biofilm EPS: Pseudomonas aeruginosa	$1 - 10^3$	$10^{-2} - 10^{6}$	$10^{-6} - 10^{5}$	(13,20,21,23,30,38–43)
Biofilm EPS: Staphylococcus epidermidis	1 - 10	$10^{-2} - 10^{6}$	$10^{-6} - 10^{3}$	(22,24,30,38–43)

Mucus yield stress values are drawn from studies with human and porcine lung and gastric mucus, and biofilm extracellular polymeric substance (EPS) yield stress values are drawn from studies of Pseudomonas aeruginosa and Staphylococcus epidermidis. External stress for mucus is taken to be that arising from coughing, phasic breathing, mechanical ventilation, digestion, and ciliary clearance. External stresses for biofilms include examples of coughing, blood flow, mechanical agitation from tooth brushing, mixed bioreactors, and shear cleaning of biofouling on ship hulls.

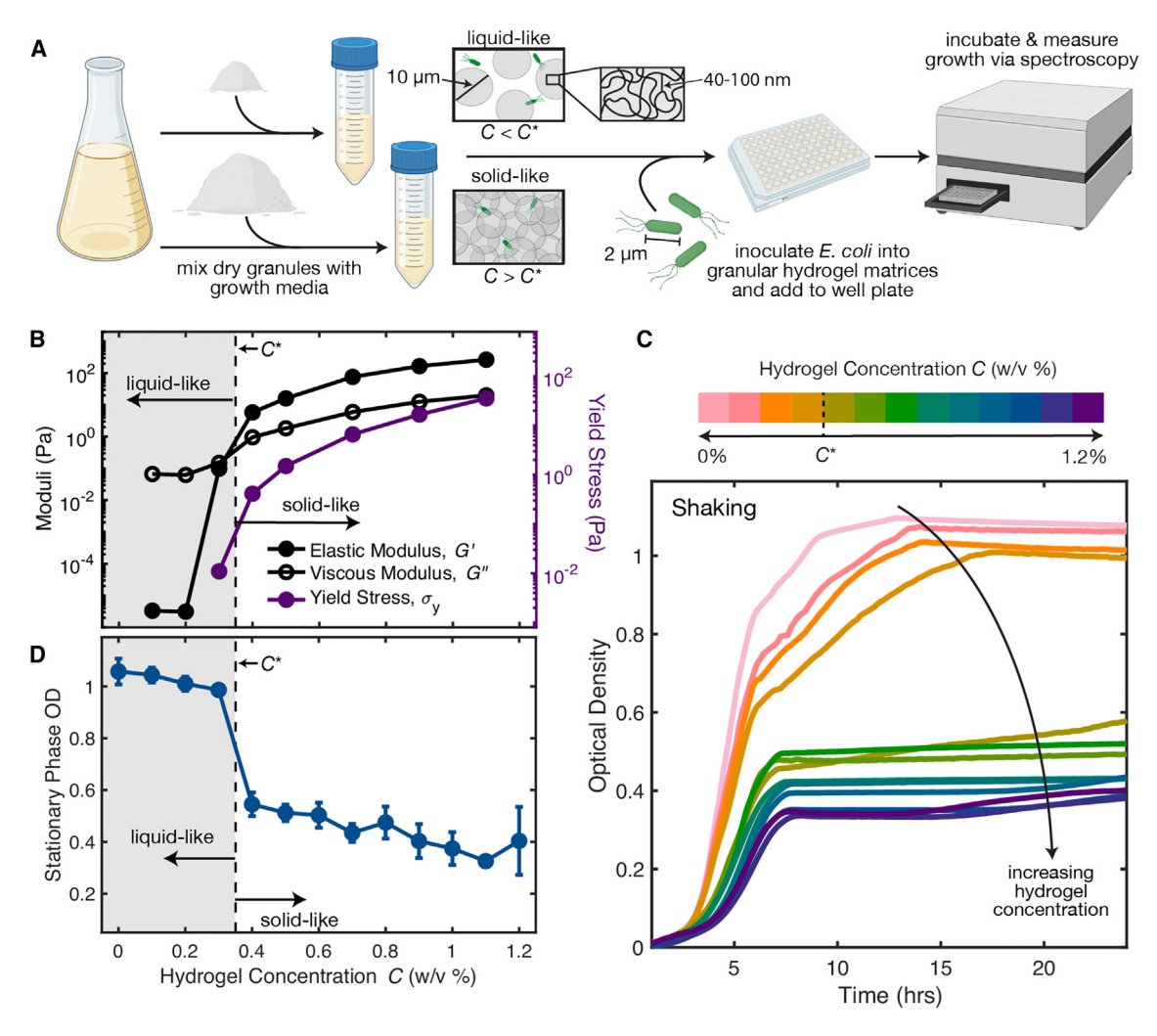


FIGURE 1 Bacterial growth is tuned by environmental rheology. (A) Schematic showing an overview of the experiments. (Left) We prepare granular hydrogel matrices by mixing dry hydrogel granules with liquid growth media at prescribed mass fractions C. (Middle) The individual granules swell to form permeable microgels whose internal mesh permits growth substrates to freely diffuse but acts as a solid barrier that confines cells. Tuning C, and therefore how closely packed the swollen microgels are, enables us to tune the overall rheological properties of the hydrogel matrices. (Right) In each hydrogel matrix, we disperse a dilute inoculum of E. coli in the interstitial voids between microgels and use spectroscopy to measure subsequent bacterial growth over 24 h under shaken or nonshaken conditions. As shown by the shear rheology measurements in (B), for small  $C < C^*$ , the dilute suspension of microgels is liquidlike; the yield stress  $\sigma_v$  (purple symbols) is below the measurement resolution, and the viscous loss modulus G'' (per black symbols) exceeds the elastic storage modulus G' (filled black symbols). By contrast, when  $C > C^*$ , the microgels are jammed, and the packing is solid-like;  $\sigma_v$ , G', and G'' all precipitously increase as C increases above the jamming concentration  $C^*$ , and G' > G''. (C) E. coli growth curves measured using spectrophotometry under shaken conditions in granular hydrogel matrices with varying C. Color bar denotes the hydrogel concentration where each color change corresponds to a 0.1% change in C. Each curve is an average of 3–5 replicates from 1 experiment. The bacteria follow a complete growth curve for  $C < C^*$  (pink to orange), but growth is arrested when  $C > C^*$  (brown to purple). (D) The transition between complete and arrested growth is summarized by plotting the stationary phase optical density, defined as the average  $OD_{600}$  from t = 18 - 24 h of the growth curves, as a function of C. The stationary phase  $OD_{600}$  drops abruptly as C increases above  $C^*$ . Error bars represent standard deviation from replicates across > 3 independent experiments. To see this figure in color, go online.

The swollen microgels are  $\sim$ 5–10  $\mu$ m in diameter with  $\sim$ 20% polydispersity but have an internal mesh size of ~40-100 nm, which permits growth substrates such as amino acids, glucose, and oxygen to freely diffuse throughout while impeding cellular motion (26). Our experiments use matrices of different mass fractions of dry granules, C (w/v %), resulting in different packing fractions of the swollen microgels-ranging from dilute suspensions with a small  $\sigma_{y}$  as described further below to tightly jammed packings with a large  $\sigma_v$  (schematized in the middle of Fig. 1 A). Hence, our approach yields hydrogel matrices whose microstructures do not limit the ability of cells to access small molecules but whose macroscopic rheological properties can be systematically tuned to mimic bacterial environments.

#### Rheology of granular hydrogel matrices

A unique feature of our hydrogel matrices is that their rheological characteristics can be dramatically altered by a small change in microgel concentration (26,27)—enabling us to probe the limits of small and large  $\sigma_v$  by varying the mass fraction C. We quantify these characteristics with an Anton Paar (Graz, Austria) MCR501 shear rheometer, loading ~2 mL of each dispersion in the 1 mm gap between two roughened 50-mm-diameter parallel circular plates. In particular, for each matrix, we use unidirectional steady-shear rheology to measure the variation of the shear stress  $\sigma$  with shear rate  $\dot{\gamma}$  (Fig. S1). For sufficiently large  $\sigma > \sigma_{\nu}$ , each matrix is fluidized, and  $\sigma$  increases with increasing  $\dot{\gamma}$ ; extrapolating to  $\dot{\gamma} \rightarrow 0$  by averaging the measured shear stress for  $\dot{\gamma} < 3 \times 10^{-3} \text{ s}^{-1}$  then provides an estimate for  $\sigma_{\nu}$ . Our measurements are summarized by the purple circles in Fig. 1 B. Matrices with small C (indicated by the gray shading) are liquid-like; their yield stress is below or near the rheometer measurement resolution, characteristic of a dilute suspension of swollen microgels. By contrast, just above  $C = C^* \approx 0.35\%$ , the matrices become solid-like, and  $\sigma_v$  increases precipitously-indicating that the microgels are sufficiently densely packed to form a jammed packing. We identify the transition between these two rheological regimes as the jamming concentration,  $C^*$ , shown by the dashed line in Fig. 1 B (26,27). As C continues to increase above  $C^*$ ,  $\sigma_v$  increases, as is characteristic of jammed packings. The values of  $\sigma$  range from  $\sim 10^{-2}$  to  $\sim 10^2$  Pa—spanning the range of yield stresses encountered by bacteria in many natural habitats (Table 1).

As a further corroboration of this rheological jamming transition, we use oscillatory rheology to measure the linear elastic storage and viscous loss moduli G' and G'', respectively, of each matrix (Fig. S2). The variation of both moduli at a fixed strain amplitude of 1% and a fixed oscillation frequency of 1 Hz with C is shown by the black circles in Fig. 1 B; these values are chosen so that the measurements are independent of strain amplitude (Fig. S2 A) and oscillation frequency (Fig. S2 B). Consistent with our expectation (26,27), G'' (open circles) exceeds G' (filled circles) for matrices with  $C < C^*$ , indicating that viscous dissipation dominates over the storage of elastic stresses-that is, these matrices are liquid-like. By contrast, for matrices with  $C \ge C^*$ , G' exceeds G'', indicating that the network of intergrain contacts and deformations of individual grains can support the applied stress and dominate the rheological response; these matrices are solid-like.

### Measuring aerobic bacterial growth

How do bacteria grow within matrices of different  $\sigma_y$ ? Notably, due to the high degree of microgel swelling and small polymer concentration ( $C \leq$ 1.2%), our granular hydrogel matrices are transparent. Therefore, we directly probe the growth and proliferation—hereafter referred to as "growth" for brevity—of E. coli using UV-visible spectroscopy (Biotek Epoch 2 microplate spectrophotometer; Winooski, VT, USA) starting with a dilute suspension of cells uniformly dispersed between the microgels (Fig. 1A).

To achieve this starting condition, prior to each experiment, we pick a single colony from an agar plate and grow it in liquid EZ Rich for 24 h in a 37°C shaking incubator. The next day, we dilute the overnight culture to an optical density (OD) of  $\sim$ 1.5. We then inoculate 3–5 mL of each test granular hydrogel matrix in a conical tube 1:100 with 30-50 µL of the diluted overnight culture and uniformly mix the cells throughout using vigorous shaking, marking t = 0 h for the subsequent growth curves. We remove the bubbles introduced by mixing by centrifuging at 3000 RCF for 10 s. Then, we gently deposit 200  $\mu$ L of each inoculated matrix into the cylindrical wells of a 96-well cell culture plate (Corning, Kennebuck, ME, USA) using a pipette or 1 mL syringe for liquid-like or solid-like matrices, respectively. We also aliquot sterile replicates of each hydrogel matrix without E. coli to use as a "blank" reference  $OD_{600}$  for each C.

We then characterize the full bacterial growth curve by incubating the microplate at 37°C for 24 h, measuring UV-visible absorption at 600 nm (OD<sub>600</sub>) every 10-15 min. To test the influence of dynamic forcing on growth, some experiments are performed shaken, in which the microplate undergoes continuous linear shaking at 567 cycles per min over a distance of 3 mm, while others are nonshaken, static cultures. We represent the growth curves (Figs. 1 C and 2, A and C) by plotting the blank-subtracted  $OD_{600}$  over time. The stationary phase  $OD_{600}$  of each sample is given by the average value of the blank-subtracted OD<sub>600</sub> 18-24 h after inoculation. The growth rate of each sample is given by the slope of  $log_2(OD_{600})$  between 1.5 and 3.5 h after inoculation, and the lag time is defined as the time at which the blank-subtracted OD<sub>600</sub> value reaches 0.02.

To validate the stationary phase OD<sub>600</sub> measurements obtained using the aerobic microplate reader, we also measure the number density of colonyforming units (per mL) for stationary phase cell cultures in granular hydrogel matrices of different concentrations. To do so, we first grow E. coli for 24 h in the matrices in microplate wells under both shaken and nonshaken conditions, as described above. We then extract ≈20-80  $\mu$ L from the center of each microplate well for serial dilution and plating and verify the pipetted volumes of these samples using mass measurements (OHAUS PA84C, Parsippany, NJ, USA) assuming a density of  $\approx 1$  g/mL. Next, we serially dilute these samples by factors of 10 in phosphate-buffered saline and plate three 10 µL droplets of each dilution on plates made of 2% Lennox LB Broth (Sigma-Aldrich, St. Louis, MO, USA) and 1.5% agar (Sigma-Aldrich). We incubate the plates at 30°C overnight before counting individual colonies the following morning. The results thereby obtained (Fig. S3) show good agreement with the results obtained using OD<sub>600</sub> measurements (Fig. 2 B); in both cases, we observe a discontinuous transition in growth between two states for shaken cultures of increasing hydrogel concentration C, whereas growth is not sensitive to C for nonshaken cultures.

# Measuring anaerobic bacterial growth

To test the influence of oxygen availability on bacterial growth within the granular hydrogel matrices, we also measure growth curves under anaerobic conditions. To do so, we use a Biotek 800 TS Absorbance Microplate Reader contained within a temperature-controlled Coy Laboratory Products (Grass Lake, MI, USA) vinyl anaerobic chamber that maintains oxygen concentrations below 60 ppm, which corresponds to ~0.03% of atmospheric oxygen at sea level. The experimental procedure, including shaking settings, is identical to that for measuring aerobic growth with one notable exception: prior to inoculation by the bacteria—which are grown aerobically overnight—each granular matrix is purged of oxygen in the anaerobic chamber for 24 h. All subsequent steps, including inoculation and microplate preparation, are performed in the anaerobic chamber. Additionally, the anaerobic absorbance reader reads OD at 630 nm instead of 600 nm. As shown in Fig. S4, OD measurements performed on the same liquid bacterial cultures using both aerobic and anaerobic microplate readers are linearly proportional; we therefore use this proportionality to convert the anaerobic OD<sub>630</sub> measurements to OD<sub>600</sub>. Similar to aerobic growth curves, the stationary phase OD<sub>600</sub> of each sample is given by the average value of the blank-subtracted OD<sub>600</sub> 18-24 h after inoculation. The growth rate of each sample is given by the slope of log<sub>2</sub>(OD<sub>600</sub>) between 2.5 and 4.5 h after inoculation, and the lag time is defined as the time at which the blanksubtracted OD<sub>600</sub> value reaches 0.02.

# Probing oxygen limitations using confocal microscopy

It is well established that newly synthesized GFP requires > 0.06% of molecular oxygen to complete fluorophore formation and emit an appreciable fluorescent signal (64-66). We use this oxygen dependence to probe the spatial distribution of oxygen in the different experiments. To do so, we repeat both shaking and nonshaking growth experiments with glass-bottom 96-well plates (Cellvis, Sunnyvale, CA, USA) for nonmotile E. coli constitutively expressing GFPmut2 in C=0.2% and 0.6%. For shaking experiments, plates were incubated in the Biotek Epoch 2 Absorbance Reader at 37°C with identical shaking conditions to growth experiments. For nonshaking experiments, cells were incubated in a stationary incubator at 37°C. After ≈20 hours of growth, we remove the plates from their incubation condition and use a Nikon A1R+ inverted laser-scanning confocal microscope to acquire vertical stacks of planar fluorescence and bright-field images, each separated by 2.5  $\mu m$  in depth, near the bottom surface of each well. We then report the average GFP fluorescence intensity of the planar image 15  $\mu$ m above the bottom surface for each replicate in Fig. 3.

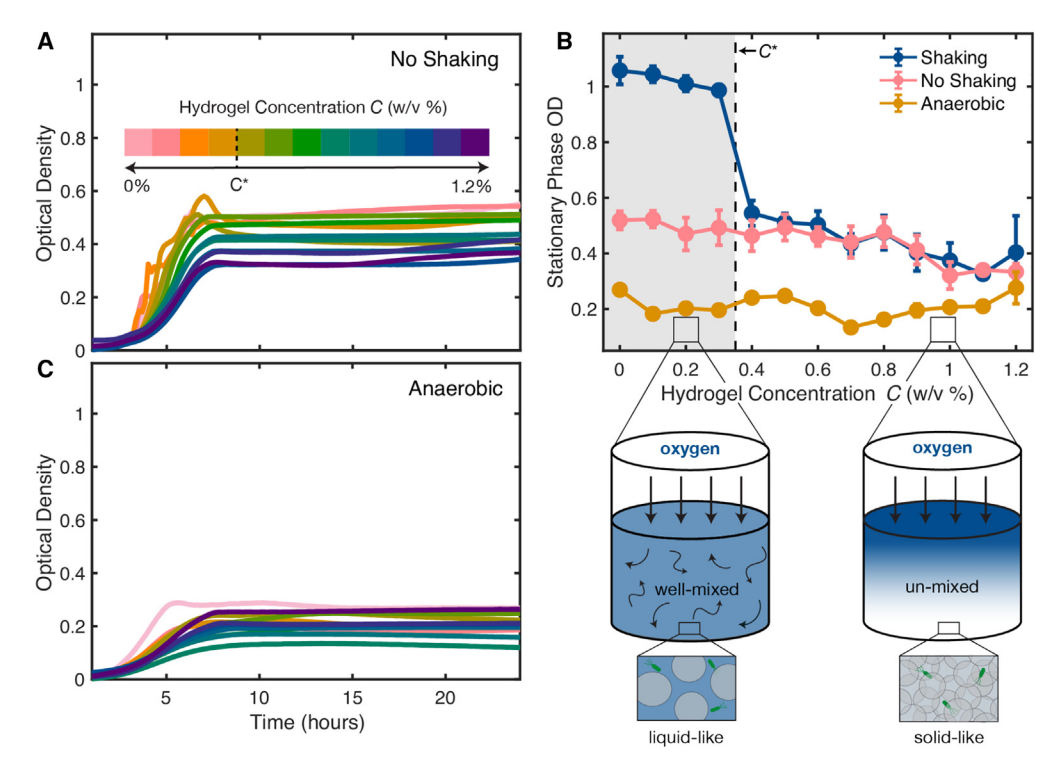


FIGURE 2 Bacterial growth is arrested across all hydrogel concentrations in nonshaken aerobic conditions and in shaken anaerobic conditions. (A) E. coli growth curves measured under nonshaken conditions in hydrogel matrices with varying C; in this case, cells exhibit arrested growth across all hydrogel concentrations (compare to Fig. 1 C). (C) E. coli growth curves measured under shaken but anaerobic conditions in hydrogel matrices with varying C; cells again exhibit arrested growth across all hydrogel concentrations. Each curve in (A) and (C) is an average of 3-5 replicates from 1 experiment. (B) These measurements are again summarized by plotting the stationary phase OD<sub>600</sub> as a function of C. While cells in shaken aerobic conditions exhibit a transition from complete to arrested growth across the jamming concentration (blue points, Fig. 1), cells in nonshaken aerobic conditions (pink) or shaken anaerobic conditions (blue) show arrested growth across all C. Error bars represent standard deviation from replicates across 2-6 independent experiments. These measurements indicate that in aerobic conditions, when shaking is sufficient to fluidize the hydrogel matrix ( $C < C^*$ ), mixing provides externally supplied oxygen to the cells and sustains complete growth (left schematic)—while in nonshaken conditions, oxygen transport is diffusion limited, and therefore cellular growth is arrested (right schematic). To see this figure in color, go online.

#### **RESULTS**

# Bacteria sharply transition to arrested growth when C exceeds C\*

We begin by examining the results of standard growth measurements performed in hydrogel-free liquid media in the wells of a 96-well cell culture plate ( $\approx$ 7 mm diameter,  $\approx$ 11 mm deep) under shaken conditions. As shown by the light pink curve in Fig. 1 C, the bacteria follow a complete growth curve with an initial lag phase (0 < t < 3 h) followed by exponential growth (3 < t < 7 h), eventually slowing down and transitioning to stationary phase as they deplete nutrients (t > 7 h). We observe similar behavior in liquidlike matrices at low hydrogel concentrations ( $0 \le C \le$ 0.3%, pink to orange curves). With progressive increases in C, cells slowly begin to transition to stationary phase earlier, yet all cultures reach similar stationary phase  $OD_{600}$  values (t > 18 h)—summarized by the points in the shaded gray region of Fig. 1 D. Surprisingly, however, further incrementing C slightly from 0.3% (C < C\*) to 0.4% ( $C > C^*$ ) results in a sharp transition to dramatically different growth behavior. As shown by the green-blue-purple curves in Fig. 1 B, despite the identical initial nutrient conditions and continuous shaking, for all C above this transition, cellular growth is slower and consistently arrested at a similarly low stationary phase cell density. This stepwise transition between continued growth and arrested growth, tuned by a slight change in hydrogel concentration across  $C^* \approx 0.35\%$ , is summarized by the stationary phase OD<sub>600</sub> values shown in Fig. 1 D and the exponential phase growth rates seen in Fig. S5 A. We observe the same phenomenon with nonmotile E. coli ( $\Delta flhDC$ ) as well (Fig. S6), suggesting that it is not linked to bacterial motility but is more general.

What causes this sharp transition from continued to arrested growth across  $C^*$ ? One possibility could be that, as C exceeds  $C^*$ , cells become physically confined in the void space between packed microgels, causing the microgels to deform and exert compressive forces that alter bacterial physiology. Direct mapping of this void space structure in 3D, detailed previously (26), indicates that this is not the case, however. In particular, the characteristic

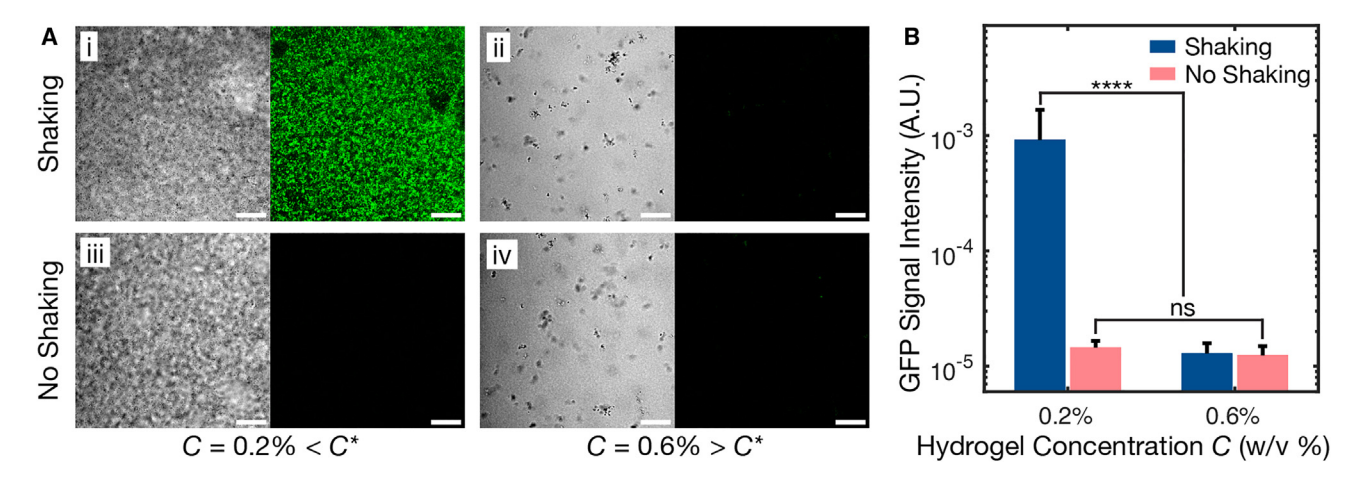


FIGURE 3 Imaging of oxygen-dependent cellular fluorescence corroborates the hypothesis schematized in Fig. 2. (A) Representative confocal bright-field (left) and fluorescence (right) microscopy images of stationary phase, nonmotile E. coli. Bright-field images show growing cells in all cases; the cells in (i) and (iii) have settled to the bottom because their matrices are unjammed, whereas the cells in (ii) and (iv) grow in small clusters because the matrix surrounding them is jammed and prevents sedimentation. The cells constitutively express GFP, which requires low levels of oxygen to fold. Only cells grown in shaken aerobic conditions in fluidized matrices with  $C < C^*$  have well-folded GFP, and therefore exhibit appreciable fluorescence, as shown in (i). Scale bar:  $50\mu m$ . (B) GFP fluorescence intensity averaged over planar images taken at a depth 15 μm above the bottom surface of each well averaged over 19–22 replicates (with error bars corresponding to the standard deviation among these replicates) confirms that the oxygen-sensitive GFP signal is significantly brighter for cells grown in shaken aerobic conditions in fluidized matrices with  $C < C^*$  (leftmost bar). Statistical significance is assessed using a one-way ANOVA test; \*\*\*\*p < 0.0001 and ns indicates a difference that is not significant. To see this figure in color, go online.

tightest size of these confining voids is larger than the size of a cell body at  $C^*$ —large enough that motile bacteria can swim through the void space, as we verified independently (25,26,67). Therefore, we expect that the cells are not appreciably compressed by the surrounding microgels at this transition. Moreover, even if slight compression of individual cells were to arise in the experiments, the matrix shear elastic modulus and yield stress at  $C^*$  are  $\sim 1$  and  $\sim 0.1$ Pa, respectively—at least 10<sup>4</sup> times smaller than the scale of the stresses at which changes in bacterial physiology have been reported to arise (51).

A related possibility could be that, due to the reduced amount of void space available to cells to grow in as C increases, crowding of cells causes them to somehow impede each other's growth. However, at  $C^*$ , the volume fraction taken up by the swollen microgels is  $\approx 64\%$ , which corresponds to random close packing of spheres; thus,  $\approx 36\%$ of the overall matrix volume corresponds to liquid-infused void space. At the onset of the transition from continued to arrested growth, the cells only take up  $\approx 0.1\%$  of this void space. Cells are thus not competing for void space at this transition. Indeed, its abrupt nature, induced by just a slight increment of C across  $C^*$ —as opposed to a smooth transition of steadily decreasing growth with increasing C, concomitant with the steady decrease in void space volume fraction and pore size—suggests that this transition does not directly arise due to the confinement of individual cells, nor is it associated with changes in the local mechanical environment encountered by individual cells, which also does not abruptly change across  $C^*$ . We therefore seek an alternate explanation of this phenomenon.

# This growth transition coincides with a sharp transition in matrix rheology

Close comparison of the data in Fig. 1, B and D, provides a clue to the underlying origin of this phenomenon: the transition between continued and arrested growth occurs when the microgels begin to jam, at which point  $(C = C^*)$  the matrices abruptly transition from being easily fluidized by shaking to tough enough to withstand shaking (detailed in materials and methods). While the flow field in each microplate well generated by linear plate reader shaking is complex, we can estimate the amplitude of the maximally imposed shaking stress using the classic solution of Stokes' second problem (68),  $\sigma \approx a \sqrt{\rho \mu \omega^3} \sim 1$  Pa, where a = 3 mm is the maximal distance traveled during shaking,  $\rho \approx 1$  g/mL is the matrix density,  $\omega \approx 10 \text{ s}^{-1}$  is the shaking frequency, and  $\mu$  is the matrix dynamic shear viscosity evaluated at a shear rate equal to  $\omega$ (Fig. S1 B). This magnitude of external stress exceeds the highest measured yield stress  $\sigma_v \lesssim 0.01$  Pa for  $C < C^*$ —hence, these matrices are fluidized by shaking, with the microgels continually rearranging and thereby promoting fluid flow and solute mixing throughout (27). By contrast, for  $C > C^*$ ,  $\sigma_{\rm v}$  approaches and then exceeds this value of  $\sigma_{\rm v}$ , indicating that these matrices remain solid-like upon shaking; the network of intergrain contacts can support the applied stress, causing individual grains to deform, but not rearrange positions with their neighbors, thereby suppressing interstitial flow and solute mixing (27). We therefore hypothesize that the transition between continued and arrested growth revealed by the experiments in Fig. 1 reflects a transition in the transport of nutrients throughout the matrices.

# The balance between shaking stress and matrix yield stress modulates mixing-induced oxygen transport, thereby regulating cellular growth

One likely candidate for a growth-limiting nutrient is oxygen—a metabolite used by E. coli to respire. These bacteria are facultative anaerobes: when oxygen is available, the cells can fully break down and utilize carbon sources via aerobic respiration, whereas when oxygen is unavailable, the cells only ferment carbon to usable energy, causing growth to become arrested compared to the aerobic case (60,61). (For this reason, E. coli are traditionally grown in shaken liquid cultures to enhance the transport of dissolved oxygen from the air head space above the culture (61–63).) Could oxygen limitations be arresting E. coli growth when the hydrogel matrix is solid-like  $(C > C^*)$ , in which case oxygen transport to the cells relies primarily on slow diffusion from the top surface of the matrix? Quantitatively, the dynamics of oxygen concentration  $c_{O_2}$  in a static matrix are described by the conservation equation  $\partial_t c_{\mathrm{O}_2} = D_{\mathrm{O}_2} \nabla^2 c_{\mathrm{O}_2} - \kappa_{\mathrm{O}_2} \rho f(c_{\mathrm{O}_2})$ , where  $D_{\mathrm{O}_2} = 2500 \, \mu\mathrm{m}^2/\mathrm{s}$  is the oxygen diffusivity,  $\kappa_{\mathrm{O}_2} \approx 1.2 \times$  $10^{-12}$  mM (cells/mL)<sup>-1</sup> s<sup>-1</sup> is the maximal oxygen uptake rate per cell (69), and  $f(c_{O_2})$  describes the influence of oxygen availability on uptake rate via Michaelis-Menten kinetics, taken to be  $\approx 1$  for simplicity, and we estimate  $\rho \approx$ 10<sup>9</sup> cells/mL using the maximal value at stationary phase for  $C > C^*$ . Solving this equation along the 1D coordinate describing the depth into the matrix from its aerated surface then yields an estimate for the characteristic depth to which oxygen diffuses before it is completely taken up by cells (70):  $l_{\rm O_2} \approx \sqrt{D_{\rm O_2} c_{\rm sat}}/(\kappa_{\rm O_2} \rho) \approx 600 \ \mu \text{m}$ , where  $c_{\rm sat} = 180 \ \mu \text{M}$  is the saturated level of dissolved oxygen (71). This depth is  $\sim$ 10 times smaller than the matrix height, and the corresponding oxygen depletion time is  $t_{\rm O_2} \approx l_{\rm O_2}^2/(D_{\rm O_2}) \approx 150$  s, far shorter than the time at which the slowdown and eventual arrest in growth become apparent in our experiments ( $\approx 4$  h). That is, when the hydrogel matrix is tough enough to withstand shaking  $(C > C^*)$  and thus oxygen availability is diffusion limited (bottom right schematic in Fig. 2), we expect that  $\sim$ 90\% of the matrix volume rapidly becomes anoxic, causing the cells therein to transition to slower, arrested growth.

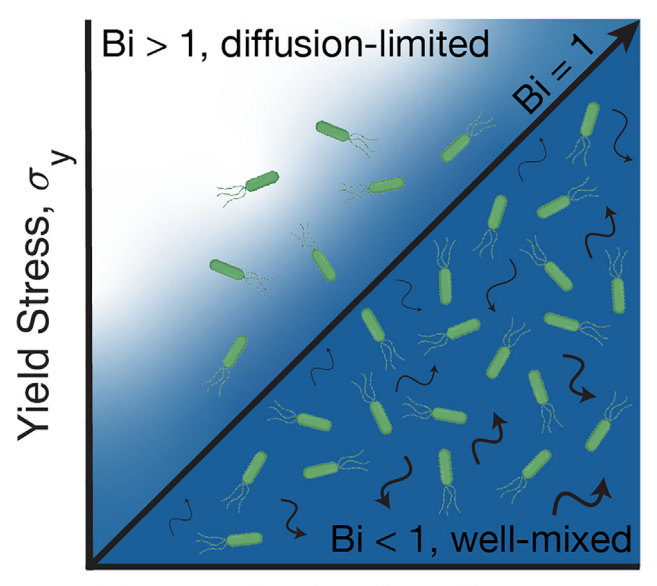
This conceptual picture makes a testable prediction: that under nonshaken conditions ( $\sigma = 0$ ), oxygen availability will always be diffusion limited, and thus bacterial growth will be similarly slow and arrested even when  $C < C^*$ . To test this prediction, we repeat the same growth experiments but without shaking. As expected, in this case, we do not see a sharp transition from continued to arrested growth with increasing C across  $C^*$ ; instead, bacteria in all the different matrices show similar slow, arrested growth curves, as shown in Fig. 2 A. As summarized by the pink circles in Figs. 2 B and S5 A, all stationary phase  $OD_{600}$  measurements and exponential phase growth rates at  $C > C^*$ collapse on top of those taken under shaken conditions, shown by the blue circles, indicating that growth is similarly arrested across these hydrogel concentrations.

As another test of this picture, we repeat the same growth experiments, with shaking, but in an anaerobic chamber where oxygen is absent. In this case, we again expect that bacterial growth will be slow and arrested for all C; indeed, we expect even slower growth compared to the previous experiments, where oxygen could still diffuse from the top surface of the matrix. Consistent with our expectation, bacteria in all the different matrices of different C show similar slow, arrested growth curves, as shown in Fig. 2 C. Moreover, as summarized by the yellow circles in Figs. 2 B and S5 A, all stationary phase OD<sub>600</sub> and exponential phase growth rate measurements, respectively, are consistent across all values of C and are even lower than those in the experiments conducted in aerobic external settings. Furthermore, the lag times for cultures to reach exponential growth following inoculation do not vary across hydrogel concentration or growth condition (Fig. S5 B), indicating that changes observed in stationary phase  $OD_{600}$  are a result of impeded exponential growth without sufficient oxygen access rather than growth timing delays.

As a final test of our picture, we take advantage of the fact that newly synthesized GFP requires oxygen to fold properly and exhibit fluorescence (64–66). Hence, to directly probe cellular growth and oxygen availability in the hydrogel matrices, we repeat both shaking and nonshaking experiments for  $C = 0.2\% > C^*$  and  $C = 0.6\% < C^*$  using nonmotile E. coli (to eliminate any confounding effects of aerotaxis) that constitutively express GFP. After  $\sim$ 20 h of growth, well into the transition into stationary phase, we use confocal microscopy to visualize cell growth and GFP fluorescence at the bottom of each matrix. The results are shown in Fig. 3 A. As expected, the only condition exhibiting an appreciable GFP signal is that of shaken unjammed matrices (i), for which  $\sigma > \sigma_v$ . The other conditions (ii–iv) all have  $\sigma < \sigma_v$ —jammed matrices are tough enough to be unmixed in both shaken (ii) and nonshaken (iii) conditions, as well as nonshaken unjammed matrices (iv)—and hence have limited oxygen availability, corroborated by the lack of GFP signal. These observations are quantified in Fig. 3 B. Taken altogether, these results demonstrate that the balance between the yield stress and external stress modulates bacterial growth by varying oxygen transport to the cells.

#### **DISCUSSION**

By probing E. coli growth inside permeable 3D granular hydrogel matrices, we have shown that the balance between the yield stress  $\sigma_{v}$  and external stress  $\sigma$  can modulate bacterial growth by altering transport of externally supplied nutrients. This balance can be quantified using Bi  $\equiv \sigma_v/\sigma$ , a dimensionless parameter used in the field of rheology



# Externally Applied Stress, $\sigma$

FIGURE 4 State diagram describing how the balance between environmental yield stress  $\sigma_v$  and the external stress  $\sigma$  modulates bacterial growth by modulating nutrient transport. When cells inhabit fragile environments that are fluidized by external forcing (bottom right), nutrients (blue) are well mixed over large length scales, and cellular growth can progress completely. By contrast, when cells inhabit tough environments that are not fluidized (top left), nutrients are not well mixed, and their availability is diffusion limited, arresting cellular growth. The boundary between these two growth regimes is described by the diagonal line, Bi  $\equiv \sigma_y/\sigma = 1$ . As shown in Table 1, natural bacterial communities inhabit settings that span both regimes of this state diagram. To see this figure in color, go online.

(72), as summarized in Fig. 4. In particular, our experiments demonstrate that when the cells inhabit strongly forced (large  $\sigma$ ) and easily fluidized (small  $\sigma_v$ ), and thus wellmixed over large length scales, environments, nutrients are more readily available to the cells, and their growth can progress completely (Bi < 1 shown in the bottom right of Fig. 4). By contrast, when the cells inhabit weakly forced (small  $\sigma$ ) and tough (large  $\sigma_v$ ) environments, slow diffusion from external boundaries limits the availability of growthlimiting nutrients, and cellular growth is arrested (Bi > 1 shown in the *top left* of Fig. 4). The transition between these two different growth behaviors across Bi = 1 can be remarkably sharp as a function of small changes in rheology, as shown in Fig. 1, C and D. This mechanism by which environmental rheology modulates bacterial physiology by altering large-scale nutrient transport does not arise from local mechanical interactions, unlike other mechanisms (46–54,56–59); instead, it likely operates in conjunction with them.

The conceptual picture described above, and schematized in Fig. 4, focuses on nutrient transport over large length scales. However, we note that even when Bi < 1, nutrient transport can still be limited by diffusion over small length scales. This limitation can be quantified using another dimensionless parameter—the Péclet number. This quantity compares the rates of nutrient transport by advective mixing of the fluidized environment under external forcing,  $\sim u/L$ , and diffusion,  $\sim D/L^2$ : Pe  $\equiv uL/D$ , where u is the characteristic advection speed, L is the characteristic length scale of nutrient transport from its source to the cells, and D is the nutrient diffusivity. That is, nutrient transport is dominated by advective mixing—as assumed above—when the characteristic distance from a nutrient source to the cells  $L \ge D/u$ . By contrast, if Pe < 1 even when Bi < 1, then we expect that nutrient transport will be diffusion limited as in the Bi > 1 case. For our experiments,  $Pe \ge 1$  for all length scales ≥80 nm, nearly two orders of magnitude smaller than the height of our hydrogel matrices and, indeed, smaller than an individual cell itself-thus, nutrient transport does indeed occur primarily by advection in our experiments when Bi < 1. However, one could imagine other scenarios involving much slower-diffusing nutrients or weaker external forcing in which, even for Bi < 1, L < D/u and nutrient transport to the cells is still diffusion limited. Exploring this possibility will be a useful direction for future work.

Our experiments used plate reader shaking as a way of testing the influence of external forcing. They also used tunable granular hydrogel matrices as well-defined and well-characterized model materials to test the influence of environmental rheology, enabling us to explore a broad range of Bi in a well-defined and systematic manner. Moreover, as an illustrative example, we used ambient oxygen as a growth-limiting nutrient for cells that grow more efficiently via aerobic respiration. However, natural settings may present additional complexities in, e.g., the nature of external forcing, the microstructure and chemical properties of the bacterial environment, and the biochemical properties of the nutrient. Nevertheless, we expect that our central finding, summarized by Fig. 4, applies more generally across different forms of forcing, microbial cell types, and nutrient sources in diverse environments where growthlimiting nutrients are not uniformly abundant. In fact, given that bacterial habitats (e.g., mucus in the body, extracellular polymer networks in biofilms) have such widely varying rheological properties and encounter diverse forms of external forcing (e.g., mechanical agitation, imposed fluid flows), Bi spans a broad range of values from much smaller to much larger than one in natural and industrial settingsas summarized in Table 1. Exploring the generality of our findings through experimental measurements of yield stresses, externally imposed stresses, and growth behavior across diverse bacterial types and environments will therefore be a useful direction for future work.

While our study focused on overall bacterial growth, we conjecture that the interplay between environmental yielding and external forcing can modulate other aspects of bacterial physiology as well. For example, we showed that when Bi > 1, nutrient availability is limited by the

competition between diffusion and uptake by cells, with greater limitation for slower diffusion and/or faster uptake, respectively. Under these conditions, nutrients are distributed heterogeneously throughout space, potentially driving collective migration and nonuniform spatial organization of cells in a population (73,74). Such "patchy" nutrient availability can also promote the establishment of phenotypic and genotypic heterogeneity, as well as competition and cooperation via metabolic cross-feeding, in a population (75)—with implications for, e.g., the maintenance of genetic diversity in the population, as well as its resilience to external stressors such as administered antibiotics (76–79). Investigating how our findings may translate to other such changes in bacterial physiology will be an interesting avenue for future research.

#### **SUPPORTING MATERIAL**

Supporting material can be found online at https://doi.org/10.1016/j.bpj. 2024.03.008.

#### **AUTHOR CONTRIBUTIONS**

A.M.H. and S.S.D. designed the experiments; A.M.H. performed all experiments; A.M.H. and S.S.D. designed and performed theoretical calculations; A.M.H. and S.S.D. analyzed all data, discussed the results and implications, and wrote the manuscript; and S.S.D. designed and supervised the overall project.

#### **ACKNOWLEDGMENTS**

We thank Christopher Browne, Jenna Moore-Ott, and Victoria Muir for useful discussions, the lab of Mohamed Donia for allowing use of the anaerobic chamber, and the lab of Howard Stone for allowing use of the roughened parallel plates for rheology. This work was supported in part by the National Science Foundation Graduate Research Fellowship Program (to A.M.H.) under grant no. DGE-2039656, Princeton University's Materials Research Science and Engineering Center under NSF grant no. DMR-2011750, and partial support from NSF grants CBET-1941716, DMR-2011750, and EF-2124863. Any opinions, findings, and conclusions or recommendations expressed in this material are those of the authors and do not necessarily reflect the views of the National Science Foundation. This work was also supported in part by a Camille Dreyfus Teacher-Scholar Award from the Camille and Henry Dreyfus Foundation, the Pew Biomedical Scholars Program, and the Princeton Catalysis Initiative.

#### **DECLARATION OF INTERESTS**

The authors declare no competing interests.

# **REFERENCES**

- 1. Bjarnsholt, T., P. Ø. Jensen, ..., N. Høiby. 2009. Pseudomonas aeruginosa biofilms in the respiratory tract of cystic fibrosis patients. Pediatr. Pulmonol. 44:547–558. https://doi.org/10.1002/ppul.21011.
- 2. Stoodley, P., S. F. Conti, ..., S. Kathju. 2011. Characterization of a mixed MRSA/MRSE biofilm in an explanted total ankle arthroplasty.

- FEMS Immunol. Med. Microbiol. 62:66-74. https://doi.org/10.1111/j. 1574-695X.2011.00793.x.
- 3. Stoodley, P., L. Nistico, ..., S. Kathju. 2008. Direct demonstration of viable Staphylococcus aureus biofilms in an infected total joint arthroplasty: a case report. J. Bone Joint Surg. Am. 90:1751-1758. http:// journals.lww.com/00004623-200808000-00019.
- 4. Zaat, S. A. J., C. A. N. Broekhuizen, and M. Riool. 2010. Host tissue as a niche for biomaterial-associated infection. Future Microbiol. 5:1149-1151. https://doi.org/10.2217/fmb.10.89.
- 5. Ribet, D., and P. Cossart. 2015. How bacterial pathogens colonize their hosts and invade deeper tissues. Microb. Infect. 17:173-183. https:// linkinghub.elsevier.com/retrieve/pii/S1286457915000179.
- 6. Gill, C. O., and N. Penney. 1977. Penetration of bacteria into meat. Appl. Environ. Microbiol. 33:1284–1286. https://doi.org/10.1128/ aem.33.6.1284-1286.1977.
- 7. Shirai, H., A. K. Datta, and S. Oshita. 2017. Penetration of aerobic bacteria into meat: a mechanistic understanding. J. Food Eng. 196:193-207. https://linkinghub.elsevier.com/retrieve/pii/S0260877416303739.
- 8. Langendries, S., and S. Goormachtig. 2021. Paenibacillus polymyxa, a jack of all trades. Environ. Microbiol. 23:5659-5669. https://doi.org/ 10.1111/1462-2920.15450.
- 9. Adadevoh, J. S. T., C. A. Ramsburg, and R. M. Ford. 2018. Chemotaxis increases the retention of bacteria in porous media with residual NAPL entrapment. Environ. Sci. Technol. 52:7289-7295. https://doi.org/10. 1021/acs.est.8b01172.
- 10. Decho, A. W., and T. Gutierrez. 2017. Microbial extracellular polymeric substances (EPSs) in ocean systems. Front. Microbiol. 8:922. https://doi.org/10.3389/fmicb.2017.00922/full.
- 11. Ratkovich, N., W. Horn, ..., T. R. Bentzen. 2013. Activated sludge rheology: A critical review on data collection and modelling. Water Res. 47:463–482. https://linkinghub.elsevier.com/retrieve/pii/S0043135412008330.
- 12. Narayanan, C. M., and V. Narayan. 2019. Biological wastewater treatment and bioreactor design: a review. Sustain. Environ. Res. 29:33. https://doi.org/10.1186/s42834-019-0036-1.
- 13. Gloag, E. S., G. K. German, ..., D. J. Wozniak. 2018. Viscoelastic properties of Pseudomonas aeruginosa variant biofilms. Sci. Rep. 8:9691. https://www.nature.com/articles/s41598-018-28009-5.
- 14. Kavishvar, D., and A. Ramachandran. 2023. The yielding behaviour of human mucus. Adv. Colloid Interface Sci. 322, 103049.
- 15. Birket, S. E., K. K. Chu, ..., S. M. Rowe. 2014. A functional anatomic defect of the cystic fibrosis airway. Am. J. Respir. Crit. Care Med. 190:421-432. https://doi.org/10.1164/rccm.201404-0670OC.
- 16. Patarin, J., É. Ghiringhelli, ..., M. Robert de Saint Vincent. 2020. Rheological analysis of sputum from patients with chronic bronchial diseases. Sci. Rep. 10, 15685. https://www.nature.com/articles/s41598-020-72672-6.
- 17. Celli, J. P., B. S. Turner, ..., S. Erramilli. 2007. Rheology of gastric mucin exhibits a pH-dependent sol-gel transition. Biomacromolecules. 8:1580-1586. https://doi.org/10.1021/bm0609691.
- 18. Boucher, R. C., C. U. Cotton, ..., J. R. Yankaskas. 1988. Evidence for reduced Cl- and increased Na+ permeability in cystic fibrosis human primary cell cultures. J. Physiol. 405:77-103.
- 19. Yan, J., A. Moreau, ..., H. A. Stone. 2018. Bacterial biofilm material properties enable removal and transfer by capillary peeling. Adv. Mater. 30, 1804153.
- 20. Körstgens, V., H. C. Flemming, ..., W. Borchard. 2001. Influence of calcium ions on the mechanical properties of a model biofilm of mucoid Pseudomonas aeruginosa. Water Sci. Technol. 43:49-57.
- 21. Körstgens, V., H.-C. Flemming, ..., W. Borchard. 2001. Uniaxial compression measurement device for investigation of the mechanical stability of biofilms. J. Microbiol. Methods. 46:9-17. https:// linkinghub.elsevier.com/retrieve/pii/S0167701201002482.
- 22. Pavlovsky, L., J. G. Younger, and M. J. Solomon. 2013. In situ rheology of Staphylococcus epidermidis bacterial biofilms. Soft Matter. 9:122-131. http://xlink.rsc.org/?DOI=C2SM27005F.

- 23. Greener, J., W. Y. Harvey, ..., S. J. Charette. 2022. Critical shear stresses of Pseudomonas aeruginosa biofilms from dental unit waterlines studied using microfluidics and additional magnesium ions. Phys. Fluids, 34.
- 24. Di Stefano, A., E. D'Aurizio, ..., L. Cellini. 2009. Viscoelastic properties of Staphylococcus aureus and Staphylococcus epidermidis monomicrobial biofilms. Microb. Biotechnol. 2:634-641.
- 25. Bhattacharjee, T., and S. S. Datta. 2019. Bacterial hopping and trapping in porous media. Nat. Commun. 10:2075. http://www.nature.com/ articles/s41467-019-10115-1.
- 26. Bhattacharjee, T., and S. S. Datta. 2019. Confinement and activity regulate bacterial motion in porous media. Soft Matter. 15:9920-9930. http://xlink.rsc.org/?DOI=C9SM01735F.
- 27. Bhattacharjee, T., C. P. Kabb, ..., T. E. Angelini. 2018. Polyelectrolyte scaling laws for microgel yielding near jamming. Soft Matter. 14:1559-1570. http://xlink.rsc.org/?DOI=C7SM01518F.
- 28. Ghanem, R., P. Roquefort, ..., T. Montier. 2021. Apparent yield stress of sputum as a relevant biomarker in cystic fibrosis. Cells. 10:3107. https://www.mdpi.com/2073-4409/10/11/3107.
- 29. Ghadiali, S. N., and D. P. Gaver. 2008. Biomechanics of liquid-epithelium interactions in pulmonary airways. Respir. Physiol. Neurobiol. 163:232-243. https://linkinghub.elsevier.com/retrieve/pii/S1569904808001006.
- 30. Button, B., H. P. Goodell, ..., M. Rubinstein. 2018. Roles of mucus adhesion and cohesion in cough clearance. Proc. Natl. Acad. Sci. USA. 115:12501–12506. https://doi.org/10.1073/pnas.1811787115.
- 31. Nucci, G., B. Suki, and K. Lutchen. 2003. Modeling airflow-related shear stress during heterogeneous constriction and mechanical ventilation. J. Appl. Physiol. 95:348-356. https://doi.org/10.1152/japplphysiol.01179.2001.
- 32. Chowdhary, R., V. Singh, ..., A. B. Gupta. 1999. Relationship of flow and cross-sectional area to frictional stress in airway models of asthma. J. Asthma. 36:419-426.
- 33. Tarran, R., B. Button, ..., R. C. Boucher. 2005. Normal and cystic fibrosis airway surface liquid homeostasis: the effects of phasic shear stress and viral infections. J. Biol. Chem. 280:35751-35759.
- 34. Bottier, M., S. Blanchon, ..., B. Louis. 2017. A new index for characterizing micro-bead motion in a flow induced by ciliary beating: Part I, experimental analysis. PLoS Comput. Biol. 13, e1005605.
- 35. Yates, G. T., T. Y. Wu, ..., C. L. Frand. 1980. A theoretical and experimental study on tracheal muco-ciliary transport. Biorheology. 17:151-162.
- 36. Abrahamsson, B., A. Pal, ..., J. G. Brasseur. 2005. A novel in vitro and numerical analysis of shear-induced drug release from extendedrelease tablets in the fed stomach. Pharm. Res. (N. Y.). 22:1215-1226.
- 37. Li, Y., and F. Kong. 2022. Simulating human gastrointestinal motility in dynamic in vitro models. Compr. Rev. Food Sci. Food Saf. 21:3804-3833.
- 38. Modaresi, M. A., and E. Shirani. 2023. Mucociliary clearance affected by mucus-periciliary interface stimulations using analytical solution during cough and sneeze. Eur. Phys. J. A. 138:201-218.
- 39. Oh, M. J., A. Babeer, ..., H. Koo. 2022. Surface topography-adaptive robotic superstructures for biofilm removal and pathogen detection on human teeth. ACS Nano. 16:11998-12012. https://doi.org/10. 1021/acsnano.2c01950.
- 40. Menesses, M., J. Belden, ..., J. Bird. 2017. Measuring a critical stress for continuous prevention of marine biofouling accumulation with aeration. Biofouling. 33:703-711. https://doi.org/10.1080/08927014. 2017.1359574.
- 41. Kamensky, K. M., A. M. Hellum, ..., P. H. Moisander. 2020. Underwater shear-based grooming of marine biofouling using a non-contact Bernoulli pad device. Biofouling. 36:951-964. https://doi.org/10. 1080/08927014.2020.1834539.
- 42. Fagherazzi, S., and P. L. Wiberg. 2009. Importance of wind conditions, fetch, and water levels on wave-generated shear stresses in shallow intertidal basins. J. Geophys. Res. 114. 2008JF001139. https://doi. org/10.1029/2008JF001139.

- 43. Roux, E., P. Bougaran, ..., T. Couffinhal. 2020. Fluid shear stress sensing by the endothelial layer. Front. Physiol. 11:861. https://doi. org/10.3389/fphys.2020.00861/full.
- 44. Persat, A., C. D. Nadell, ..., H. A. Stone. 2015. The mechanical world of bacteria. Cell. 161:988-997.
- 45. Chawla, R., R. Gupta, ..., P. P. Lele. 2020. A skeptic's guide to bacterial mechanosensing. J. Mol. Biol. 432:523-533.
- 46. Dufrêne, Y. F., and A. Persat. 2020. Mechanomicrobiology: how bacteria sense and respond to forces. Nat. Rev. Microbiol. 18:227-240. http://www.nature.com/articles/s41579-019-0314-2.
- 47. Gordon, V. D., and L. Wang. 2019. Bacterial mechanosensing: the force will be with you, always. J. Cell Sci. 132:jcs227694. https:// journals.biologists.com/jcs/article/132/7/jcs227694/57420/Bacterialmechanosensing-the-force-will-be-with.
- 48. Cho, H., H. Jönsson, ..., A. Levchenko. 2007. Self-organization in high-density bacterial colonies: efficient crowd control. PLoS Biol. 5, e302. https://doi.org/10.1371/journal.pbio.0050302.
- 49. Ben-Ari, E. 2008. Understanding bacterial crowd control. Bioscience. 58:88. https://academic.oup.com/bioscience/article/58/1/88/233686.
- 50. You, Z., D. J. G. Pearce, and L. Giomi. 2021. Confinement-induced self-organization in growing bacterial colonies. Sci. Adv. 7, eabc8685. https://doi.org/10.1126/sciadv.abc8685.
- 51. Chu, E. K., O. Kilic, ..., A. Levchenko. 2018. Self-induced mechanical stress can trigger biofilm formation in uropathogenic Escherichia coli. Nat. Commun. 9:4087. http://www.nature.com/articles/s41467-018-06552-z.
- 52. Zhang, Q., J. Li, ..., J. Yan. 2021. Morphogenesis and cell ordering in confined bacterial biofilms. Proc. Natl. Acad. Sci. USA. 118, e2107107118. https://doi.org/10.1073/pnas.2107107118.
- 53. Delarue, M., J. Hartung, ..., O. Hallatschek. 2016. Self-driven jamming in growing microbial populations. Nat. Phys. 12:762-766.
- 54. Berg, H. C. 1993. Random Walks in Biology, expanded edition. Princeton University Press, Princeton, N.J.
- 55. Wadhwa, N., Y. Tu, and H. C. Berg. 2021. Mechanosensitive remodeling of the bacterial flagellar motor is independent of direction of rotation. Proc. Natl. Acad. Sci. USA. 118, e2024608118.
- 56. Watari, N., and R. G. Larson. 2010. The hydrodynamics of a run-andtumble bacterium propelled by polymorphic helical flagella. Biophys. J. 98:12-17. https://linkinghub.elsevier.com/retrieve/pii/ S0006349509015562.
- 57. Zöttl, A., and J. M. Yeomans. 2019. Enhanced bacterial swimming speeds in macromolecular polymer solutions. Nat. Phys. 15:554-558. http://www.nature.com/articles/s41567-019-0454-3.
- 58. Patteson, A. E., A. Gopinath, ..., P. E. Arratia. 2015. Running and tumbling with E. coli in polymeric solutions. Sci. Rep. 5, 15761. http:// www.nature.com/articles/srep15761.
- 59. Kamdar, S., S. Shin, ..., X. Cheng. 2021. The colloidal nature of complex fluids leads to enhanced motility of flagellated bacteria. Preprint at arXiv. http://arxiv.org/abs/2107.14266.
- 60. Lin, E. C., and A. S. Lynch. 2012. Regulation of Gene Expression in Escherichia coli. Springer Science & Business Media.
- 61. Losen, M., B. Frölich, ..., J. Büchs. 2004. Effect of oxygen limitation and medium composition on Escherichia coli fermentation in shakeflask cultures. Biotechnol. Prog. 20:1062-1068.
- 62. Samadi, Z., M. Mehdizadeh Allaf, ..., H. Peerhossaini. 2022. Effects of turbulent mixing and orbitally shaking on cell growth and biomass production in active fluids. Am. J. Biomed. Sci. Res. 15:396-404.
- 63. Duetz, W. A. 2007. Microtiter plates as mini-bioreactors: miniaturization of fermentation methods. Trends Microbiol. 15:469-475.
- 64. Heim, R., D. C. Prasher, and R. Y. Tsien. 1994. Wavelength mutations and posttranslational autoxidation of green fluorescent protein. Proc. Natl. Acad. Sci. USA. 91:12501-12504. https://doi.org/10.1073/pnas. 91.26.12501.
- 65. Tsien, R. Y. 1998. The Green Fluorescent Protein. Annu. Rev. Biochem. 67:509–544. https://doi.org/10.1146/annurev.biochem.67.1.509.

- 66. Vordermark, D., T. Shibata, and J. M. Brown. 2001. Green fluorescent protein is a suitable reporter of tumor hypoxia despite an oxygen requirement for chromophore formation. Neoplasia. 3:527-534. https://linkinghub.elsevier.com/retrieve/pii/S1476558601800087.
- 67. Bhattacharjee, T., D. B. Amchin, ..., S. S. Datta. 2021. Chemotactic migration of bacteria in porous media. Biophys. J. 120:3483-3497. https://linkinghub.elsevier.com/retrieve/pii/S0006349521004276.
- 68. Pereiro, I., A. Fomitcheva-Khartchenko, and G. V. Kaigala. 2020. Shake it or shrink it: Mass transport and kinetics in surface bioassays using agitation and microfluidics. Anal. Chem. 92:10187-10195. https://doi.org/10.1021/acs.analchem.0c01625.
- 69. Fu, X., S. Kato, ..., T. Emonet. 2018. Spatial self-organization resolves conflicts between individuality and collective migration. Nat. Commun. 9:2177. http://www.nature.com/articles/s41467-018-04539-4.
- 70. Martínez-Calvo, A., T. Bhattacharjee, ..., S. S. Datta. 2022. Morphological instability and roughening of growing 3D bacterial colonies. Proc. Natl. Acad. Sci. USA. 119, e2208019119.
- 71. Al-Ani, A., D. Toms, ..., M. Ungrin. 2018. Oxygenation in cell culture: Critical parameters for reproducibility are routinely not reported. PLoS One. 13, e0204269.
- 72. Coussot, P. 2016. Rheophysics. Springer.

- 73. Budrene, E. O., and H. C. Berg. 1991. Complex patterns formed by motile cells of Escherichia coli. Nature. 349:630-633.
- 74. Zhao, H., A. Košmrlj, and S. S. Datta. 2023. Chemotactic motilityinduced phase separation. Phys. Rev. Lett. 131, 118301. https://doi. org/10.1103/PhysRevLett.131.118301.
- 75. Schreiber, F., and M. Ackermann. 2020. Environmental drivers of metabolic heterogeneity in clonal microbial populations. Curr. Opin. Biotechnol. 62:202-211.
- 76. Zhang, Q., G. Lambert, ..., R. H. Austin. 2011. Acceleration of emergence of bacterial antibiotic resistance in connected microenvironments. Science. 333:1764-1767. https://doi.org/10.1126/science. 1208747.
- 77. Hermsen, R., J. B. Deris, and T. Hwa. 2012. On the rapidity of antibiotic resistance evolution facilitated by a concentration gradient. Proc. Natl. Acad. Sci. USA. 109:10775-10780. https://doi.org/10. 1073/pnas.1117716109.
- 78. Greulich, P., M. Scott, ..., R. J. Allen. 2015. Growth-dependent bacterial susceptibility to ribosome-targeting antibiotics. Mol. Syst. Biol. 11:796. https://doi.org/10.15252/msb.20145949.
- 79. Baym, M., T. D. Lieberman, ..., R. Kishony. 2016. Spatiotemporal microbial evolution on antibiotic landscapes. Science. 353:1147-1151. https://doi.org/10.1126/science.aag0822.